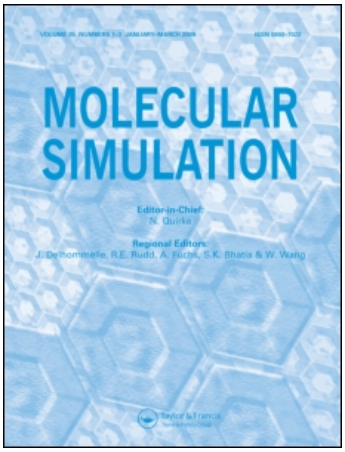

Molecular Simulation
Publication details, including instructions for authors and subscription information:
http://www.informaworld.com/smpp/title~content=t713644482

Molecular Dynamics Modelling of Polymer Materials

J. H. R. Clarke[a]; D. Brown[a]
[a] Chemistry Department, U.M.I.S.T., Manchester, UK

To cite this Article Clarke, J. H. R. and Brown, D.(1989) 'Molecular Dynamics Modelling of Polymer Materials', Molecular Simulation, 3: 1, 27 — 47
To link to this Article: DOI: 10.1080/08927028908034618
URL: http://dx.doi.org/10.1080/08927028908034618

Molecular Simulation, 1989, Vol. 3, pp. 27–47
Reprints available directly from the publisher
Photocopying permitted by license only

MOLECULAR DYNAMICS MODELLING OF POLYMER MATERIALS†

J.H.R. CLARKE and D. BROWN

Chemistry Department U.M.I.S.T., Manchester M60 1QD, UK

(*Received May 1988; in final form June, 1988*)

This paper describes novel molecular dynamics simulations of a model amorphous polymer which resembles polyethylene. Methylene groups are represented as single interaction sites and both torsional and angle bending potentials are included. New parameters for both inter- and intramolecular potentials are used as compared to previous work on alkane chains. A previously used torsional potential was found to have a serious deficiency. Dense samples of amorphous polymer were prepared using a self avoiding random walk in three dimensions carried out within the confines of periodic boundaries. For the molecular dynamics an adaptation of the method of Berendsen *et al* is presented in which changes in the shape and size allow the prepared samples to relax out significant internal stresses. This same method can be used to examine the response of a polymer sample to an externally applied stress field. An example is given of a sample undergoing uniaxial tension, and the results are discussed in terms of the elastic strain, yielding and plastic flow. The latter effect is compared with neck formation, a phenomenon which is observed in real polymeric materials.

KEY WORDS: Molecular Dynamics, Polyethylene, uniaxial tension, neck formation

INTRODUCTION

The mechanical properties of polymers are fundamental to the majority of their practical and industrial applications. Future technological developments are likely to place high demands on our basic understanding of these materials and there is a strong need for accurate prediction of properties without resorting to expensive synthesis and testing procedures. Our aim in this article is to demonstrate how molecular dynamics computer simulation techniques can contribute to this basic understanding by showing directly how the mechanical response of a dense polymer structure is related to the monomer level interactions. This offers a new approach to improving the design of polymer materials.

Much of our current understanding of the properties of polymers is based on the successful application of statistical dynamical theories to conceptually simple models which ignore the detailed structures of the individual chains [1–3]. In dense polymers, however, conformational chain fluctuations are greatly restricted by cross linking, excluded volume effects, entanglements and specific interactions such as hydrogen bonding. Various approximate models have been introduced to account for some of these effects [4] but there is increasing evidence that for a quantitative understanding of dense polymers it is necessary to take specific account of monomer level interactions.

In a previous article [5] we have described molecular dynamics simulation of amorphous and ordered microstructures of a model oriented polymer fibre using a

†Invited paper.

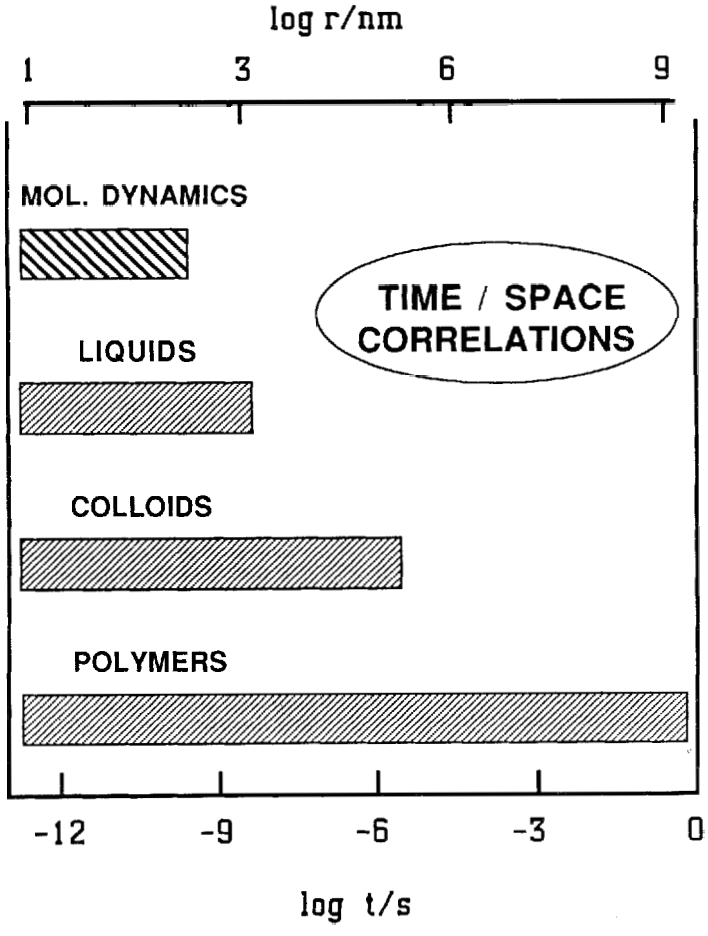

Figure 1 A schematic diagram showing the range of space and time correlations accessible using molecular dynamics and those that contribute significantly to the properties of various systems.

lamina model in which the linear chains were suspended between two parallel planes representing the faces of adjacent crystallites. The microstructures were subjected to an applied strain normal to the parallel planes. It was shown that interchain forces have quite significant indirect effects on the measured stress by restricting the configurational fluctuations of individual chains in sometimes quite subtle ways. The structures were probed at the molecular level to reveal the effects of applied stress on chain configurations, bond angle distributions, etc, which are fundamental properties of the material but which are not readily accessible in laboratory experiments.

In this article we shall concentrate attention on novel molecular dynamics simulations of a dense amorphous polymer using a constant stress molecular dynamics technique. This method makes use of three dimensional periodic boundary conditions but allows direct examination of the deformation of the microscopic sample under the influence of an externally applied tensorial pressure field.

There are certain basic requirements of any simulation if it is to be at representative of bulk behaviour.

(1) The size of the sample and the length of the simulation must be such as to contain all the important fluctuations contributing to the essential properties of the system.

(2) The structure of the sample must be compatible with the periodic boundary conditions.

(3) A suitable model must be chosen for the interaction potentials between constituent molecules.

(4) A method must be designed for preparing an equilibrium sample. For liquids this is quite straightforward but for dense polymers it is a non-trivial problem.

With current computing resources we can follow the behaviour of only small samples (< 10000 interaction sites) for short periods of time (< 1 ns) so that whatever problems are chosen then the essential aspects of the phenomena must be observable within these limitations. Figure 1 shows schematically the range of time and space correlations that are accessible using computer simulation and those that contribute significantly to the properties of various materials. Most of the properties of even moderately complicated liquids are largely determined by short range spatial correlations and processes which decay on time scales shorter than a few ns; hence the success of computer simulation studies in this area. However, the same is certainly not true in, for instance, colloids and polymers where there are some regimes e.g. in polymer solutions and melts where fluctuations covering several orders of magnitude of both wave vector and time scale make an important contribution to a wide range of properties.

Our approach to polymer simulations is to focus attention on the dense regime close to the glass transition where the situation is in many ways simplified since the slow processes in the system (e.g. diffusion) have been almost completely frozen out and where mechanical properties are, to a large extent, determined by the high frequency motions within the system.

We have adopted a model in which a *single* linear chain of N sites forms a dense amorphous polymeric system through the replicative properties of periodic boundaries. The structure is entirely consistent with the periodic boundaries with each site of the *continuous* chain either being in the primary cell or in a neighbouring cell. For small N there is no doubt that such a model gives a poor representation of bulk behaviour but as N becomes larger we expect it to be an increasingly better approximation to a dense amorphous polymeric system. A similar model has been used by Weber [6] to simulate an infinite chain. In the present model, however, the shape of the periodic cell is permitted to deform in order to relax internal stress imbalances.

In the next sections we shall describe interaction potentials and the methods used to synthesize a dense polymer sample. We also give details of the "constant" stress MD technique used for these polymer samples and discuss some preliminary results on mechanical deformation of a polymer resembling polyethylene.

INTERACTION POTENTIALS

Three essential features of linear chain molecules are built into the model – connectiv-

ity, chain flexibility and van der Waals interactions between monomers. The choice of parameters is such that the chains *resemble* the linear hydrocarbon polymer polyethylene (PE). In previous simulations of polymer microstructure we used a model adapted from simulations of low molecular weight alkanes preferring to concentrate attention on the general relation between bulk and microscopic properties [5]. Some adjustments have now been made to the potentials in the light of our previous results, on the basis of some recent theoretical work [7] and also by means of some simple comparisons with data on PE [8]. These changes rectify some of the more obvious deficiencies. We have not embarked on an exhaustive search for the optimum parameters since this would divert attention away from the main aim of trying to gain a better general understanding of the mechanical properties of polymeric systems.

In the model we have used each monomer unit is treated as a single site and is given a mass corresponding to that of a CH_2 group. Neighbouring sites on the chain are connected together by rigid bonds of length $b_0 = 0.153$ nm. Flexibility of the chains is achieved by incorporating a harmonic valence angle potential, $\Phi(\theta)$, and a torsional potential, $\Phi(\alpha)$, into the model. $\Phi(\theta)$ is of the form.

$$\Phi(\theta) = \tfrac{1}{2} k_\theta(\cos\theta - \cos\theta_0)^2 \quad (1)$$

where $k_\theta = 520\,\mathrm{kJ\,mol^{-1}}$ and $\theta_0 = 112.813°$. The torsional potential restricting internal rotations about a bond in the chain is parametrised in terms of the dihedral angle, α, formed by this bond and the two adjacent bonds. The exact form used is that due to Steele [7] and is given below

$$\Phi(\alpha)/\mathrm{J\,mol^{-1}} = C_0 + C_1\cos\alpha + C_2\cos^2\alpha + C_3\cos^3\alpha \quad (2)$$

where $C_0 = 8832$, $C_1 = 18087$, $c_2 = 4880$ and $C_3 = 31800$. Finally, non-bonded monomer interactions, i.e. those between sites separated by at least three others, are represented by a Lennard-Jones (LJ) 12–6 potential with $\varepsilon/k_B = 72\,\mathrm{K}$[9] and $\sigma = 0.428$ nm.

In our previous simulations of fibre microstructure [5] we used an older form of torsional potential [10] which incorporates explicit coupling between bond angle bending and the torsional motions. Although some coupling is to be expected its extent in the above model is now believed to be unrealistic. Recent work using this potential has revealed a disproportionately high rate of gauche–gauche barrier crossings – $\sim$6 times more frequent than gauche–trans transitions. Although this may partly be due to the low value of k_θ used in the original parametrisation, increasing k_θ by a factor of four to the value given above only reduced the rate of gauche–gauche transitions to $\sim\frac{1}{8}$ of the gauche–trans rate which is still much higher than obtained with potentials where there is no coupling. Consequently in the absence of quantitative experimental data on the form of the coupling we have resorted to using a torsional potential which is solely a function of the dihedral angle. The one given in eqn. 2 is that fitted by Steele [7] to his data obtained from a fairly comprehensive *ab initio* treatment of the torsional potential in butane. The potential is compared in Figure 2 with the potential used in I and also with the potential proposed by Ryckaert and Bellemans [11] on the basis of older data.

Parameters used for the valence angle potential are significantly different to those used in I. θ_0 has been changed to the value given by Steele [7] and k_θ has been increased by a factor of four. This increase in k_θ is derived from our previous result for the

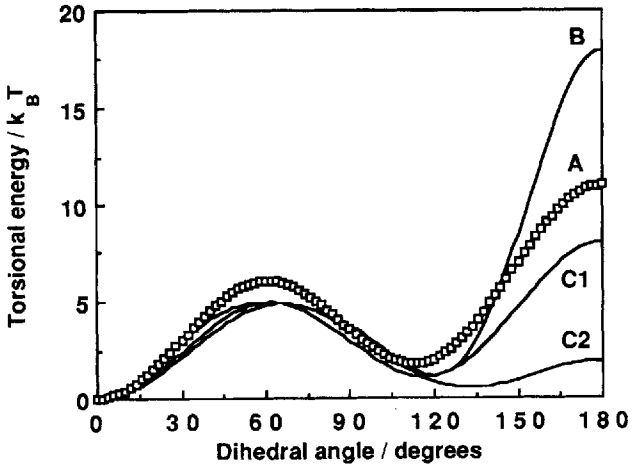

Figure 2 The torsional potential energy function, in units of $k_B T(T = 300\,K)$, plotted against the dihedral angle. The curve marked A is that given by Steele [7] and used in this paper. Curve B is that popularized by Ryckaert and Bellemans [11]. Curves C1 and C2 are for the one we have used previously [5] with the valence angle set equal to the equilibrium value and also to 120° respectively. Note the reduction in the gauche–gauche barrier.

Young's modulus of crystalline PE which was about a quarter of the known value [12]. According to the analysis of Treloar [13] the Young's modulus should be linearly dependent upon the valence angle bending force constant when the bonds are rigid.

For the interchain potential LJ site–site interactions are used but the value of σ has been increased to 0.428 nm to give a density of $\sim 0.85\,g\,cm^{-3}$ at 300 K and 1 bar which is the value expected on the basis of extrapolations of the liquid part of the phase diagram [8]. Note that an actual comparison with the experimental density is quite difficult as in reality PE forms partially-crystalline solids containing varying amounts of amorphous material depending upon many factors.

"CONSTANT STRESS" MOLECULAR DYNAMICS

We have used a method described originally by Berendsen *et al* [14] which involves weak coupling of an external tensorial pressure field, $\mathbf{P}_0$, to the system through a simple feedback loop. It is assumed that provided the coupling is loose enough it will have an insignificant effect on the first order properties of the system. The coupling is implemented by allowing the matrix **h**, made up from the basis vectors, **a**, **b** and **c** which determine the shape of the primary dynamics cell, to respond to imbalances between the internally measured pressure tensor and an externally applied pressure tensor. We have modified the original method to ensure that **h** remains symmetric throughout by defining the equation for the rate of change of the **h** matrix with time to be

$$\dot{\mathbf{h}} = \frac{\mathbf{P} - \mathbf{P}_0}{M} \tag{3}$$

where M is a constant and **P** is the internally measured pressure tensor, which in this case is defined to be symmetric,

$$\mathbf{P} = \frac{1}{V}\sum_{i=1}^{N}\left[\frac{1}{m_i}\mathbf{p}_i\mathbf{p}_i + \mathbf{r}_i\mathbf{f}_i\right] \tag{4}$$

where the volume, V, is calculated from the determinant of the matrix **h**,

$$V = 8*\det \mathbf{h} = 8\mathbf{a}\cdot(\mathbf{b}\times\mathbf{c}) \tag{5}$$

The factor of 8 appearing as in our calculations the origin for the basis vectors is the centre of the primary cell. In keeping with the loose coupling method [14] and other "constant pressure" schemes [15, 16] a simple proportional scaling of coordinates is used to minimize local disturbances. So defining a set of scaled coordinates, **s**, by

$$\mathbf{s} = \mathbf{h}^{-1}\mathbf{r} \tag{6}$$

and differentiation gives the following equation of motion for the sites

$$\dot{\mathbf{r}}_i = \mathbf{h}\dot{\mathbf{s}}_i + \dot{\mathbf{h}}\mathbf{s}_i = \frac{\mathbf{p}_i}{m_i} + \dot{\mathbf{h}}\mathbf{h}^{-1}\mathbf{r}_i \tag{7}$$

The motion is thus seen to be split into two contributions which are integrated separately, that due to the momenta and that resulting from the change in shape and size of the cell. The "fast" motions due to the momenta are dealt with in the usual way using a "leapfrog" algorithm incorporating an iterative scheme to maintain the constraints whereas a simple first order Taylor expansion is considered sufficient to integrate the equation for the relatively "slow" motion of the box

$$\mathbf{h}(t+\Delta t) = \mathbf{h}(t) + \left[\frac{\mathbf{P}-\mathbf{P}_0}{M}\right]\Delta t \tag{8}$$

It can then simply be shown that to first order the motion of the box results in a scaling of the position of a site

$$\mathbf{r}_i(t+\Delta t) = \mathbf{h}(t+\Delta t)\mathbf{h}^{-1}(t)\mathbf{r}_i(t) = \mathbf{H}\mathbf{r}_i(t) \tag{9}$$

This method was preferred to the more rigorous Rahman-Parinello (RP) technique [16] for the following reasons. In polymers it is more natural to use an "atomic" pressure tensor, eqn. 4, in place of the centre of mass pressure tensor employed in simulations of molecular liquids [17] (for the single chain simulation described here it is essential). This means that both intrachain and interchain forces have explicitly to be considered. Since bond constraints are favoured over the use of real bond forces (for reasons of computational efficiency) this raises a problem in writing the Lagrangian of the system when the RP method is to be used. Loose coupling has some additional practical advantages. For instance the pressure imbalance is coupled to the first derivative of the basis vectors rather than to the second derivative, so that motions of the box are overdamped and there is little tendency for an unphysical oscillatory response to changes in the applied pressure.

In the experiments to be described external work is done on the samples so that in order to maintain a uniform temperature all the simulations reported here were run under isokinetic conditions using an "*ad hoc*" rescaling of momenta procedure [18]; this method is in fact a limiting case of the temperature control which is also described

by Berendsen *et al.* [14]. Details of the algorithm for the constant pressure – constant temperature simulations are given in the Appendix.

SAMPLE PREPARATION

A common method of preparing equilibrium samples of atomic liquids for computer simulations is to melt a crystal configuration. As the system melts the short correlation lengths involved and the mobility of the atoms ensure that an isotropic liquid structure is formed within a relatively short space of time. Long correlation lengths and low mobility ensure that this approach is a totally impractical way of generating a sample of amorphous polymer. Instead it is necessary to synthesize in the computer an amorphous structure that is already close to equilibrium as near to the required density as possible. For this purpose we have used a modified self-avoiding random walk performed within the confines of the periodic boundary conditions.

The method generates the linear chain sequentially site by site with an acceptance criterion very similar to the Monte Carlo method. At each step a new proposed site is generated by first of all choosing an intended dihedral angle, α, ($\alpha = 0$ implies trans), using a random number generator. The proposed position, $\mathbf{r}_{i+1}$, is then calculated from the three previous sites in accordance with the equilibrium bond length, b_0, and valence angle, θ_0, and the random dihedral angle. If the new position lies outside the primary cell then its image within the cell is calculated in the usual way. The change in energy, $\Delta\Phi$, caused by introducing this site is then determined by summing up all new interactions, using the minimum image convention, and adding to this the new contribution to the dihedral angle energy, $\Phi(\alpha)$. The Boltzmann factor of this energy change, $\exp(-\Delta\Phi/k_B T)$, is then compared to another random number between 0 and 1. If the random number is less than the Boltzmann factor then the new site is accepted, otherwise it is rejected and a new proposed site is generated. Should repeated trials fail to find an acceptable position for the new site the chain is shortened by one site and the process starts afresh by attempting to generate a new $\mathbf{r}_i$. If the chain again cannot find a suitable $\mathbf{r}_{i+1}$ then the chain is shortened this time by two sites and so on until a route is found past the blockage. This process continues until all N sites have been generated.

What criteria can be used to determine if the chain structures generated as above are at all representative of real bulk systems? Firstly we have compared the conformational distributions of samples grown at higher density with those found at low density where an ideal distribution is more likely. We have also compared the chain statistics with those expected from random walks in three dimensions. There is now widespread experimental evidence which confirms theoretical predictions that even in dense polymers there exists the same Gaussian distribution of end-to-end distances as is predicted for the isolated "ideal" chain [19]. Indeed this is one of the cornerstones of the theory of rubber elasticity [3].

In Table 1 the percentages of dihedral angles in the three possible states, defined as

$$\mathbf{G}^- \quad -180° < \alpha < -60° \quad \text{(gauche minus)} \tag{10}$$

$$\mathbf{T} \quad -60° < \alpha < +60° \quad \text{(trans)} \tag{11}$$

$$\mathbf{G}^+ \quad +60° < \alpha < +180° \quad \text{(gauche plus)} \tag{12}$$

Table 1 The percentages of dihedral angles in he three possible states, G^-, T and G^+, obtained from:-
A. a configuration generated at $\varrho = 0.001\,g\,cm^{-3}$, T = 300 K,
B. a configuration generated at $\varrho = 0.6\,g\,cm^{-3}$, T = 300 K,
C. sample B relaxed at T = 300 K, P = 1 bar, ($\langle\varrho\rangle = 0.84\,g\,cm^{-3}$).
D. the Boltzmann factor of the torsional potential.

	A	*B*	*C*	*D*
$\%G^-$	11.2	20.5	13.7	12.5
%T	75.0	63.1	73.1	74.9
$\%G^+$	13.7	16.5	13.2	12.5

are given for configurations generated both at low density ($0.001\,g\,cm^{-3}$) and at high density ($0.6\,g\,cm^{-3}$). These distributions are compared in the table to those for the higher density configuration after being equilibrated at a temperature of 300 K and an applied pressure of 1 bar and also to that determined assuming that the probability density for the dihedral angle is proportional to the Boltzmann factor of the torsional potential,

$$\varrho(\alpha) \propto \exp\left(\frac{-\Phi(\alpha)}{k_B T}\right) \tag{13}$$

From the table it can been seen that the chain generation procedure favours configurations with more dihedral angles in the gauche state as the initial density is increased. The low density "ideal" chain has a distribution very similar to that expected purely on the basis of the Boltzmann factor of the torsional potential suggesting that at this temperature the so called "pentane" effect does not have much overall influence. The relaxed structure (C) closely resembles the two "ideal" cases. The greater symmetry of this distribution compared to its initial state is an additional indication that equilibrium has been established.

According to statistical theory of chain polymers the mean squared end-to-end distance, $\langle \mathbf{r}^2 \rangle$, should be linearly dependent upon the number, n, of statistically uncorrelated subunits [20]

$$\langle \mathbf{r}^2 \rangle = na^2 \tag{14}$$

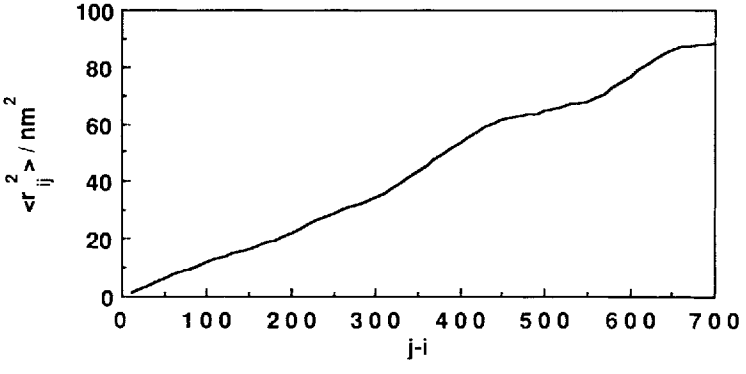

Figure 3 The mean squared site–site separation, $\langle r_{ij}^2 \rangle$, plotted as a function of the difference between the sites, j–i. Statistical theory of polymer chains predicts a linear plot.

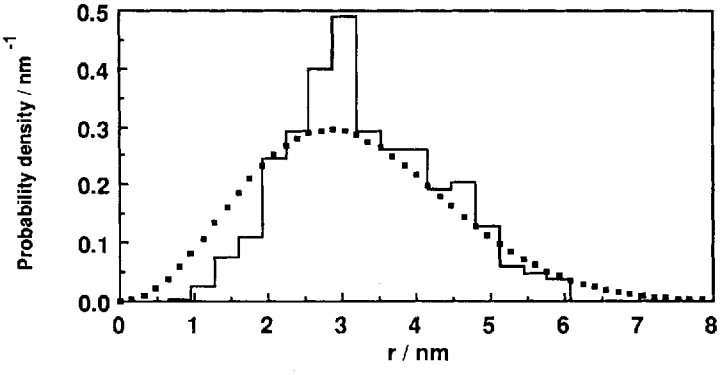

Figure 4 The probability density function for the intersite separation, $\mathbf{r}_{ij}$, for j–i = 100 for the N = 1000 site configuration referred to as B in Table 1. The theoretical distribution, Equation 15, is shown as the black squares.

and the probability density function, P(r), for the scalar distance between the ends takes the form [20]

$$P(r) = 4\pi r^2 \left(\frac{3}{2\pi\langle \mathbf{r}^2 \rangle}\right)^{3/2} \exp\left(\frac{-3r^2}{2\langle \mathbf{r}^2 \rangle}\right) \tag{15}$$

With one chain, of course, it is not easy to test this without doing very long runs but to a good approximation [21] we can use the site–site separation, $\mathbf{r}_{ij}$, for a fixed value of j–i in place of the end-to-end distance. Therefore, we have plotted $\langle \mathbf{r}_{ij}^2 \rangle$ against j–i in Figure 3 and in Figure 4 the actual density distrubiton for site–site separation distances has been compared to that predicted by equation 15 for a value of j–i = 100. In both cases the configuration of N = 1000 sites generated at 0.6 g cm^{-3}, referred to as B in Table 1, has been used. The expected linearity of the mean squared site–site distance plot is seen to hold quite well for values of j–i up to ~700. Despite the statistical limitations the comparison between the observed and theoretical distributions is reasonably favourable.

SIMULATIONS

Checks on the stability of the basic algorithm were made under conditions of constant total energy by switching off the temperature scaling and the cell deformations. It was found that time steps above ~8 fs caused the total energy to diverge but to keep the root mean square fluctuations in the total energy down to ~2% of those in the total potential energy required a time step of 5 fs, and this value was used throughout.

The value of the arbitrary coupling constant M (see equation 3) was adjusted to give a time scale of relaxation to pressure imbalances of the order of a few picoseconds, i.e. relatively slow compared to the fluctuations of components of the pressure tensor itself. The value eventually chosen was M = 2.625*10^6 Pa s m^{-1} and this was used for all the simulations reported below.

The LJ 12–6 potential was truncated at $r_c = 2.5\sigma$ and the appropriate long range corrections were made to the potential energy and the virial at each step according to

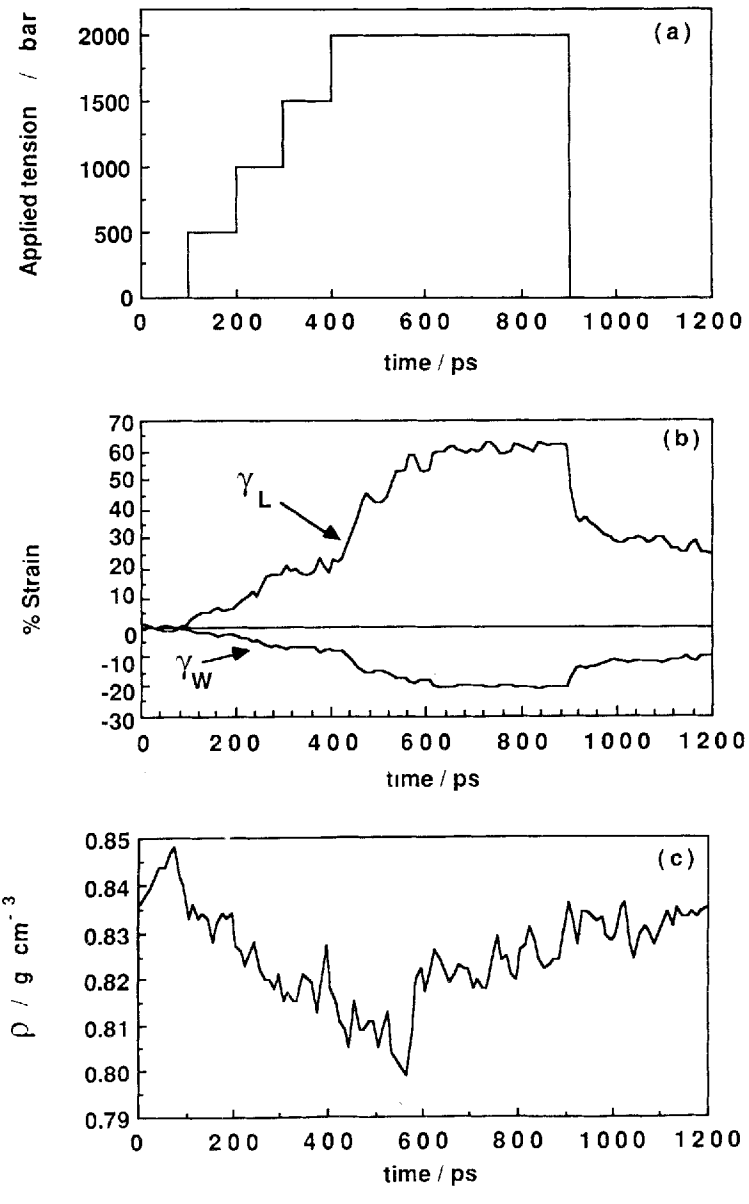

Figure 5 (a) The tension applied uniaxially along the y laboratory axis plotted as a function of time. (b) The extensile, γ_L, and contractile, γ_W, strains plotted as percentages against time. (c) The density plotted as a function of time.

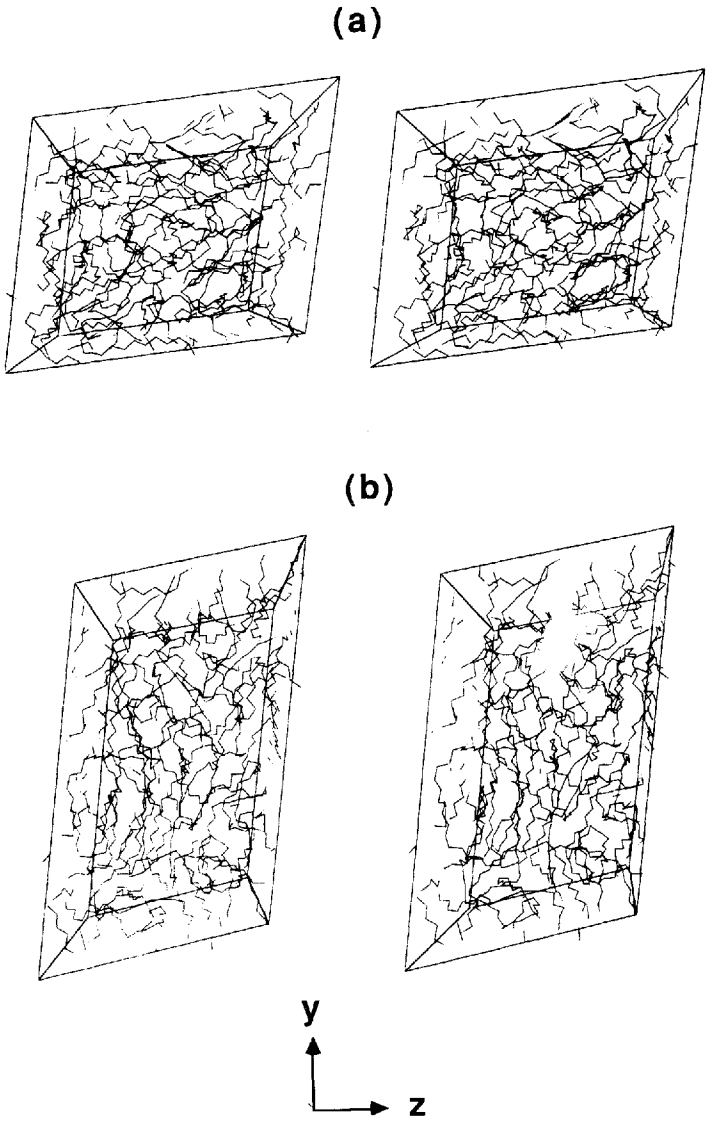

Figure 6 Stereo plots of the configuration of N = 1000 sites at (a) 100 ps into the experiment, i.e. before tension applied, and (b) 900 ps, i.e. after the sample had been under an applied tension of 2 k bar for 500 ps. Only the basic MD cell is shown.

the density and assuming $g(r) = 1$ for $r > r_c$. Comparison with more "exact" results, obtained by using a larger value for r_c of 3.5σ, revealed that the error introduced by assuming $g(r) = 1$ with $r_c = 2.5\sigma$ was of about the same order as the statistical error in the energy and the pressure due to the fluctuations in these properties. A check was also made at each step to ensure that the perpendicular distance between any of the opposite faces of the primary cell did not drop below $2r_c$. This is important as the cell

can, and certainly does, distort significantly away from its cubic origins. This is especially so when subjected to anisotropic pressure fields.

All the simulations were performed on the Cyber 205 at UMRCC with programs vectorised using methods [22] based on the algorithm of Ahlrichs and Brode [23]. For a 1000 site sample the program requires about 0.28 s of Cyber 205 CPU time per time step which represents an increase in speed by at least a factor of ten over the Cyber 176.

DYNAMIC DEFORMATION OF THE POLYMER SAMPLE

The simulation experiments described below were performed on an amorphous 1000 site chain configuration which had been relaxed at 300 K. The sample was grown at a density of 0.6 g cm $^{-3}$ and then equilibrated for 300 ps in an isotropic pressure field of 1 bar (i.e. $\mathbf{P}_0$/bar = **1**) according to the procedure described in the previous section.

The experiment was started from this point in time and the sample was subjected to the scheme of uniaxial tension, directed along the y laboratory axis, shown in Figure 5a. For the first 100 ps the sample was allowed to equilibrate further at an isotropic pressure of 1 bar, so as to gather statistics for the unperturbed chain. The applied tension was then set to 500 bar ($P_{yy_0} = -500$ bar) and then increased in a stepwise fashion by 500 bar after each subsequent 100 ps time period until the applied tension reached 2000 bar at which point the sample was allowed to "equilibrate" at this tension. After 500 ps at 2000 bar the tension was removed and the sample allowed to relax for a further 300 ps at an isotropic pressure of 1 bar.

Stereoscopic representations are shown in Figure 6 of the structure both at equilibrium and after being subjected to the uniaxial tension. The views are down the x axis of the laboratory coordinate system. It can be seen that even at equilibrium the shape of the primary cell has departed significantly from its initial cubic symmetry as a result of signifcant internal stresses generated in the originally prepared sample.

RESULTS AND DISCUSSION

In this section we give some of the results from just one experiment as an illustration of the usefulness of the method described above. We do not intend to discuss in great detail the relevance of such results with respect to the behaviour of real polymeric materials. This will be the subject of a further paper which will also include details of more comprehensive tests of the method including those on number dependence and reproducibility. This is necessary as it is more than likely that samples differing in size and/or preparational history will produce a spread of results when external pressure fields are applied.

To present, in an uncomplicated way, the complex response of the shape and dimensions of the system to the applied tension the **h** matrix has been used to calculate the length of the primary cell, L, parallel to the direction of the applied tension and the cross-sectional area, A, perpendicular to it and from A an effective width, W, can be defined

$$W = A^{1/2} \tag{16}$$

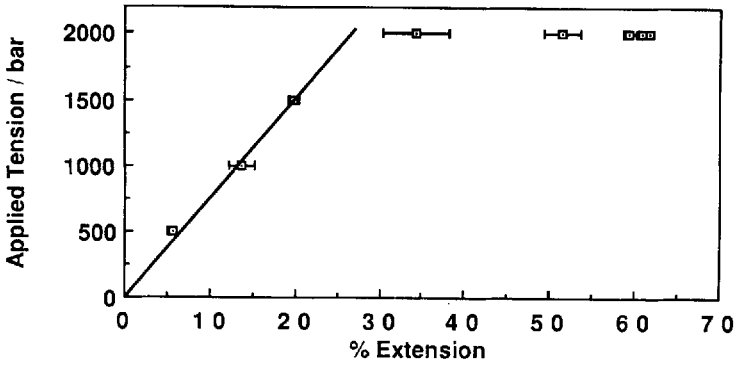

Figure 7 The percentage extension averaged over the 100 ps intervals the sample was under tension plotted against the applied tension. The straight line gives a limiting Young's modulus of ~0.7 GPa. The break in the plot occurs at the yield point.

From L and W the effect of the applied tension can be resolved into the strains parallel and perpendicular to the direction of application

$$\gamma_L = \frac{L - L_0}{L_0} \tag{17}$$

$$\gamma_W = \frac{W - W_0}{W_0} \tag{18}$$

where the zero suffix denotes the equilibrium value defined in this case as the average over the first 100 ps. These properties are plotted in terms of percentages as a function of time in Figure 5b and reveal a steady increase in the extension of the sample up to 400 ps. At this point the highest tension of 2000 bar is applied and there is a detectable break in the behaviour. The existence of a "yield point" is more evident from Figure 7 where the average strain for each of the 100 ps intervals where the sample is under tension is plotted. Up to an applied tension, τ, of 1500 bar the response is linear giving an estimate for Young's modulus, E, defined as

$$E = \frac{\tau}{\gamma_L} \tag{19}$$

of about 0.7 GPa. This compares well with an estimated value of 0.5 GPa for the Young's modulus of amorphous PE [24]. The eventual yield in the sample is strikingly similar to the well documented [25] phenomenon of "necking" in real polymeric materials. Care must be taken in making this comparison, however, since values of the macroscopic "yield stress" for polyethylene [26] are about an order of magnitude lower than the value of ~2 kbar seen here.

There are several possible reasons for the discrepancy. Firstly, our sample is totally amorphous whereas, as already stated, real PE is partially crystalline and it is well known [26] that structure has a strong influence on mechanical properties. Secondly, the microscopic size of the model sample and the boundary conditions do not permit the same form of inhomogeneous deformation. In laboratory measurements the actual tension in the vincinity of the point at which the neck originally forms are

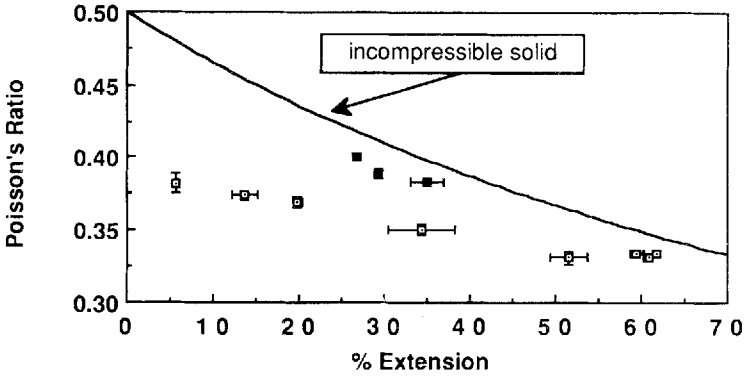

Figure 8 Poisson's ratio plotted as a function of the percentage extension. Both quantities are averaged over 100 ps intervals, whilst under tension (open squares) and after the cessation of tension (filled squares). The solid line indicates the value expected for Poisson's ratio for an incompressible material, see Equation 21.

difficult, if not impossible, to make. What is termed the "true stress" [25] can only be inferred from the cross-sectional area of the neck and the applied load. Thirdly the difference in time scales may also contribute. Studies of the strain rate dependence of the yield stress in real materials have shown [25, 27] that it increases linearly with the logarithm of the strain rate. An extrapolation using this linear hypothesis to the high strain rates used in these studies still, however, underestimates the observed yield stress. Lastly, it is very likely that the phenomenon of yield in real polymers is strongly influenced by the defects in the sample so it is then perhaps not surprising that we obtain such high values. This is certainly the case in crystalline materials [28] where simulations also give high values for shear yield stresses [29] more akin to the theoretical maximum [28] than to macroscopic values.

In many materials there exists, at least at small strains, a linear relationship between γ_W and γ_L

$$\gamma_W = -\mu\gamma_L \tag{20}$$

where μ is called Poisson's ratio. For an incompressible solid it can easily be shown that

$$\mu = \frac{1}{\gamma_L + 1 + (\gamma_L + 1)^{1/2}} \tag{21}$$

so the small strain limit is $\frac{1}{2}$. Most solids, however, undergo an increase in volume when put under tension so μ is generally low, in the range $\frac{1}{4}$ to $\frac{1}{3}$, though interestingly natural rubber has a Poisson's ratio nearer $\frac{1}{2}$ [28]. In Figure 8 Poisson's ratio is plotted against the percentage extension ($\gamma_L \times 100$) each averaged for the 100 ps intervals the system is under tension and also after the cessation of tension. Plotting the data in this way allows a comparison with the result, shown as the continuous line, expected for an incompressible material (Equation 21). At low strains μ is significantly less than that of an incompressible solid but once the system has yielded there is much more of a similarity. This is also true once the applied tension is removed.

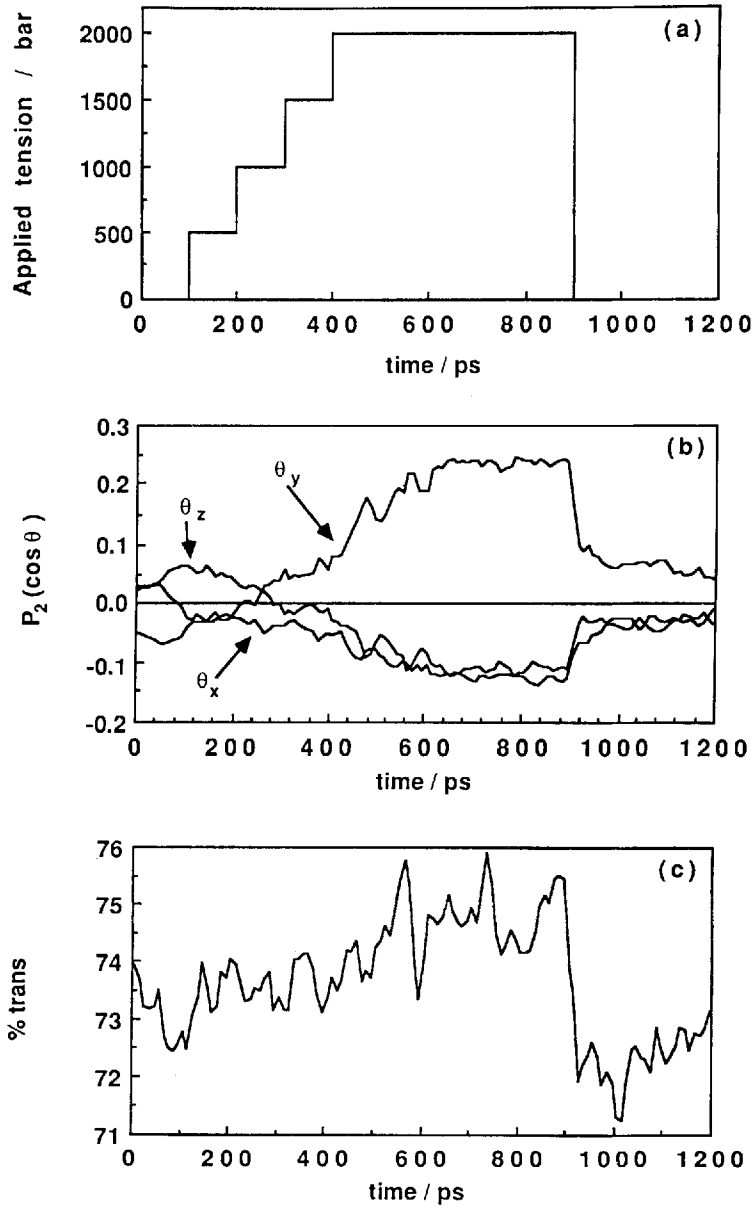

Figure 9 (a) The tension applied uniaxially along the y laboratory axis plotted as a function of time. (b) The alignment in the sample, as defined by the second order Legendre polynomial of the cosine of the angle between the chain axis and a laboratory axis (see Equation 22), plotted as a function of time. (c) The percentage of dihedral angles in the trans conformation, as defined by Equation 11, plotted against time.

The behaviour of μ as the system is put under tension implies first a drop then an increase in density, a prediction which is confirmed in Figure 5c. The break in the behaviour of the density at ~ 600 ps does not correspond to any change in the applied conditions but form Figure 5b it can be seen that it roughly coincides with the point at which the sample no longer continues to elongate. Whether the decrease in density is a necessary requirement before yielding can take place remains to be confirmed.

One of the aims of these simulation studies is to understand stress/strain behaviour in terms of changes in the chain structure. For example we now briefly discuss the chain orientation and proportion of trans conformers as a function of the applied tension; Figures 9b and 9c, respectively. We have defined the orientation of the chain by the second order Legendre polynomial of the cosine of the angle between a laboratory axis and the vector joining next-nearest neighbour sites, $\mathbf{r}_{i,i+2}$, on the chain, e.g.

$$P_2(\cos\theta_y) = \tfrac{3}{2}(\langle \cos^2\theta_{yi} \rangle - \tfrac{1}{3}) \tag{22}$$

where

$$\cos\theta_{yi} = \hat{\mathbf{y}}\cdot\hat{\mathbf{r}}_{i,i+2} \tag{23}$$

and the "hat" denotes a unit vector. The function given in eqn. 22 is experimentally measurable, using infrared spectroscopy, and the values obtained here are consistent with the results obtained for the amorphous regions of drawn high density linear polyethylene [30]. The increase in chain alignment with respect to the y axis, that along which the tension is applied, shows an almost one to one correspondence with the linear strain.

In regard to the chain conformations it can be seen that a strain of 60% is accompanied by a $\sim 2\%$ increase in the percentage of trans conformers which quickly re-equilibtrates once the tension is removed. This part of the strain is entropic in origin and is completely and rapidly recoverable. The plastic flow, or very slowly recovering, part of the strain must then be attributed to changes in the chain topology which occur under tension. Further analysis of these data will be discussed in a future article.

CONCLUSIONS

In this article we have described the preparation and molecular level simulation of a dense chain polymer under a variety of applied conditions.

The loose coupling constant stress algorithm which permits changes in both shape and size of the primary cell works satisfactorily for polymers and is essential for initial relaxation of prepared samples. It is also extremely useful for examining the mechanical response to an applied stress field. Although the method does not have the rigour of the Rahman-Parinello technique it can be used when constraint forces are included in the pressure calculation. It also gives a smooth non-oscillatory response even when large external perturbations are applied as a result of the overdamped nature of the coupling between the motion of the box and the pressure differential. This makes it extremely useful for examining mechanical properties.

Dense polymer samples were successfully synthesized using the random walk procedure and the statistical properties of the prepared configurations agreed satisfactorily with the predictions of statistical theories.

It has been demonstrated that under uniaxial tension a sample of just 1000 sites shows the elastic, yielding and non-equilibrium plastic flow type behaviour characteristic of real amorphous polymers. The Young's modulus is in reasonable agreement with the known values of polyethylene although the yield stress is an order of magnitude greater. This discrepancy is largely attributed to the fact that the sample is effectively "defect" free though other factors may also contribute as well.

Acknowledgements

We wish to thank Dr. Hawthorne Davis and Dr. Mike Wilding for valuable discussions during the course of this work, E.I. DuPont de Nemours & Co. Inc. for financial assistance and the S.E.R.C. for the provision of supercomputer time.

APPENDIX

In this Appendix we outline the implementation of the "constant pressure" method discussed in the text. The incorporation of such a scheme into the integration of the equations of motion of a system containing constraints via the leapfrog form of the Verlet algorithm is relatively straightforward and is based on that given previously [14]

We start with the coordinates of the N sites on the chain $\mathbf{r}(t)$ where $(\mathbf{r}_{i+1} - \mathbf{r}_i)^2 = b_0^2$, the corresponding momenta divided by mass at the previous half time step $\mathbf{v}\left(t - \frac{\Delta t}{2}\right)$ and the matrix of basis vectors $\mathbf{h}(t) = (\mathbf{a}\ \mathbf{b}\ \mathbf{c})$. From eqn. 5 $\mathbf{h}(t)$ determines the volume V(t) and hence the density. We refer to the vector $\mathbf{v}$ as a momenta divided by mass in preference to the term "velocity" as it is important to distinguish the motion due to the forces from that due to the changing shape of the primary cell. Velocity could be interpreted as meaning $\dot{\mathbf{r}}$ which is not the same as $\mathbf{v}$.

The procedure is as follows:-

(1) First of all we calculate the scaled positions $\mathbf{s}(t)$ of the sites of the chain within the primary cell, i.e. $-1 \leqslant \mathbf{s}(t) \leqslant 1$, using the following sequence of operations

$$\mathbf{s}(t) = \mathbf{h}^{-1}(t)\mathbf{r}(t) \tag{A1}$$

$$\mathbf{s}'(t) = \mathbf{s}(t) - 2*\mathrm{AINT}(\mathbf{s}(t)/2) \tag{A2}$$

$$\mathbf{s}(t) = \mathbf{s}'(t) - 2*\mathrm{AINT}(\mathbf{s}'(t)) \tag{A3}$$

where by AINT we refer to the FORTRAN function which returns the integer part of the expression in the bracket as a REAL variable. Note that both steps (A2) and (A3) are required as the coordinates of the continuous chain may lie some distance from the primary cell.

(2) Using the scaled coordinates the site–site separation vectors are calculated using the nearest image convention for those sites deemed to interact via the LJ 12–6 potential, thus

$$\mathbf{s}_{ij}(t) = \mathbf{s}_i(t) - \mathbf{s}_j(t) \tag{A4}$$

$$\mathbf{s}'_{ij}(t) = \mathbf{s}_{ij}(t) - 2*\mathrm{AINT}(\mathbf{s}_{ij}(t)) \tag{A5}$$

$$\mathbf{r}_{ij}(t) = \mathbf{h}(t)\mathbf{s}'_{ij}(t) \tag{A6}$$

(3) Calculate the force, $\mathbf{f}_{ij}(t)$, between sites i and j from the derivative of the LJ potential and the separation vector and also the contribution to the pressure tensor of these non-bonded forces

$$V(t)\mathbf{P}_{ss}(t) = \sum_{i} \sum_{j>i} \mathbf{r}_{ij}(t)\mathbf{f}_{ij}(t) \tag{A7}$$

where the double sum is over all interacting pairs and store the total force on each site at this point in a second vector $\mathbf{f}^{\Phi}(t) = \mathbf{f}(t)$.

(4) Calculate the forces on the sites due to the torsional and valence angle potentials, eqns. 1 and 2.

(5) From the $\mathbf{v}\left(t - \frac{\Delta t}{2}\right)$ calculate an approximation to the on step temperature, T(t), using

$$T(t) = \frac{\sum_{i=1}^{N} m_i \mathbf{v}_i^2\left(t - \frac{\Delta t}{2}\right)}{k_B N_f} \tag{A8}$$

where N_f is the total number of degrees of freedom in the system.

(6) From T(t) obtain the temperature scaling factor, λ

$$\lambda = \left[\frac{T_0}{T(t)}\right]^{1/2} \tag{A9}$$

(7) Calculate the new unconstrained positions using the leapfrog algorithm incorporating the temperature scaling factor

$$\mathbf{r}'_i(t + \Delta t) = \mathbf{r}_i(t) + \left[\lambda_i\left(t - \frac{\Delta t}{2}\right) + \frac{\mathbf{f}_i(t)}{m_i}\Delta t\right]\mathbf{v}\Delta t \tag{A10}$$

Note. Although the form of the scaling factor in Equation A9 is equivalent to using $\tau_T = \Delta t$ in Berendsen *et al's* loose loose coupling constant temperature method we do not think it appropriate to call it such when the coupling is so tight that the approximations made to allow its implementation become invalid. We prefer to refer to this form of constraint on the system as an *ad hoc* constant temperature method and as such, like other similar schemes, its effect is known to be imperceptible on the first order properties of the system [18]. The reasons for maintaining a tight control on the temperature are discussed in the text.

(8) Using an iterative scheme determine the new constrained positions ($\mathbf{r}(t + \Delta t)$) and from these the constraint forces

$$\mathbf{f}_i^c = \frac{m_i[\mathbf{r}_i(t + \Delta t) - \mathbf{r}'_i(t + \Delta t)]}{\Delta t^2} \tag{A11}$$

and the new momenta

$$m_i \mathbf{v}_i\left(t + \frac{\Delta t}{2}\right) = \frac{m_i[\mathbf{r}_i(t + \Delta t) - \mathbf{r}_i(t)]}{\Delta t} \tag{A12}$$

(9) Calculate the actual position of a site within the primary cell from the scaled positions within the primary cell

$$\mathbf{r}'(t) = \mathbf{h}(t)\mathbf{s}(t) \tag{A13}$$

and then use these to compute the contribution to the pressure tensor from the bonded forces

$$V(t)\mathbf{P}_{bf}(t) = \sum_{i=1}^{N} \mathbf{r}_i'(t)\left[\mathbf{f}_i(t) - \mathbf{f}_i^{\Phi}(t)\right] \tag{A14}$$

where $\mathbf{f}_i$ is now the total force on a site including the forces of constraint, Equation A11. The forces due to the LJ potential are subtracted as their contribution has already been calculated, Equation A7. The use of the coordinates within the primary cell for calculating $\mathbf{P}_{bf}$ maintains consistency with the calculation of $\mathbf{P}_{ss}$.

(10) From $\mathbf{v}\left(t + \frac{\Delta t}{2}\right)$ we can approximate the on-step kinetic contribution to the pressure tensor as

$$V(t)\mathbf{P}_{kin}(t) = \sum_{i=1}^{N} m_i \mathbf{v}_i\left(t + \frac{\Delta t}{2}\right)\mathbf{v}_i\left(t + \frac{\Delta t}{2}\right) \tag{A15}$$

and thus obtain the total pressure tensor

$$\mathbf{P}(t) = \mathbf{P}_{kin}(t) + \mathbf{P}_{bf}(t) + \mathbf{P}_{ss}(t) \tag{A16}$$

Note. The approximation used for the kinetic contribution to the pressure introduces an error similar to that used in calculating the temperature. Previous results [18] show that this latter error is very small. This combined with the fact that the coupling to the external tensorial pressure field is weak means that the approximation does not cause any significant problem.

(11) Update the **h** matrix using Equation 8

$$\mathbf{h}(t + \Delta t) = \mathbf{h}(t) + \left[\frac{\mathbf{P} - \mathbf{P}_0}{M}\right]\Delta t \tag{A17}$$

(12) Calculate the tensor scaling factor

$$\mathbf{H} = \mathbf{h}(t + \Delta t)\mathbf{h}^{-1}(t) \tag{A18}$$

(13) Scale the new constrained positions using **H**

$$\mathbf{r}_i'(t + \Delta t) = \mathbf{H}\mathbf{r}_i(t + \Delta t) \tag{A19}$$

(14) Return to (1) and use $\mathbf{r}'(t + \Delta t)$, $\mathbf{v}\left(t + \frac{\Delta t}{2}\right)$ and $\mathbf{h}(t + \Delta t)$.

In using Equation A19 in step 13 we are following the method as previously set out [14]. An alternative step would be

$$\mathbf{r}_i'(t + \Delta t) = \mathbf{r}_i(t + \Delta t) + (\mathbf{H} - \mathbf{1})\mathbf{r}_i(t) \quad \text{(A20)}$$

where the pressure scaling has been applied to the positions at time t rather than to the new constrained positions at $t + \Delta t$, as seems natural from a factorization of the motion into that due to the forces and that caused by the change in the shape of the cell. We have not tried this alternative formulation but do not expect it to make any difference to the results as the looseness of the coupling ensures that the displacement due to the change in the cell shape is relatively small.

This point is important since step (13) destroys the constraints. It is true that at the next step the constraints are reimposed but only after all the forces have been computed from these unconstrained positions. For potentials of the valence angle bending and torsional variety there is in principle a problem for the following reason. When deriving the forces from these potentials it is expedient to include any constraints, bond lengths for example, explicitly from the outset, thus, simplifying the resultant expression. The violation of this constraint in principle invalidates the expression for the force from these three and four body potentials. In practice, however, the constraints are only ever satisfied to within some specified tolerance so there is always some error. In a conventional (N, V, E) simulation it is possible to optimize the tolerance to give good energy conservation without spending inordinate amounts of time iterating. Throughout the simulations reported here the tolerance for the bond length constraint is set to 10^{-6} and typically the application of the scaling tensor **H** effectively reduces this to about 10^{-5}. No rigorous checks are possible in these non-conservative simulations. What can be said is that the simulations are stable and the results sensible.

References

[1] P.J. Flory, *Statistical Mechanics of Chain Molecules*, Wiley, New York, 1969.

[2] P.J. Flory, "Statistical thermodynamics of random networks," *Proc. Roy. Soc. Lond. A*, **351**, 351 (1976).

[3] L.R.G. Treloar, *The Physics of Rubber Elasticity*, 3rd ed., Oxford University Press, 1975.

[4] L.M. Dossin and W.W. Graessley, "Rubber elasticity of well-characterized Polybutadiene networks," *Macromolecules*, **12**, 123 (1979).

[5] D. Brown and J.H.R. Clarke, "Molecular dynamics computer simulation of polymer fibre microstructure," *J. Chem. Phys.*, **84**, 2858 (1986).(Note that the values of the potential parameters k_χ and ε' published in this reference were incorrect. The actual values used were 36.784 and 0.1089 kJ mol^{-1}, respectively.)

[6] T.A. Weber and F. Helfand, "Molecular dynamics simulation of polymers. I Structure," *J. Chem. Phys.*, **71**, 4760 (1979).

[7] D. Steele, "An *ab initio* investigation of the torsional potential function on n-butane," *J. Chem. Soc. Farad. Trans. II*, **81**, 1077 (1985).

[8] M.J. Richardson, P.J. Flory and J.B. Jackson, "The crystallization and melting of copolymers of polymethylene," *Polymer*, **4**, 221 (1964).

[9] J.-P. Ryckaert and A. Bellemans, "Molecular dynamics of liquid alkanes," *Farad. Disc. Chem. Soc.*, **66**, 95 (1978).

[10] T.A. Weber, "Simulation of n-butane using a skeletal alkane model," *J. Chem. Phys.*, **69**, 2347 (1978).

[11] J.-P Ryckaert and A. Bellemans, "Molecular dynamics of liquid n-butane near its boiling point," *Chem. Phys. Letts.*, **30**, 123 (1975).

[12] L. Holliday and J.W. White, "The stiffness of polymers in relation to their structure," *Pure Appl. Chem.*, **25**, 545 (1971).

[13] L.R.G. Treloar, "Calculations of elastic moduli of polymer crystals: I. Polyethylene and Nylon 66," *Polymer*, **1,** 95 (1960).
[14] H.J.C. Berendsen, J.P.M. Postma, W.F. van Gunsteren, A. DiNola and J.R. Haak, "Molecular dynamics with coupling to an external bath," *J. Chem. Phys.*, **81,** 3684 (1984).
[15] H.C. Andersen, "Molecular dynamics simulations at constant pressure and/or temperature," *J. Chem. Phys.*, **72,** 2384 (1980).
[16] M. Parinello and A. Rahman. "Crystal structure and pair potentials: A molecular dynamics study," *Phys. Rev. Letts.*, **45,** 1196 (1980).
[17] J.-P. Ryckaert and G. Ciccotti, "Introduction of Andersen's demon in the molecular dynamics of systems with constraints," *J. Chem. Phys.*, **78,** 7368 (1983).
[18] D. Brown and J.H.R. Clarke, "A comparison of constant energy, constant temperature and constant pressure ensembles in molecular dynamics simulations of atomic liquids," *Mol. Phys.*, **51,** 1243 (1984).
[19] P.J. Flory, "Molecular theory of rubber elasticity," *Polymer Journal*, **17,** 1 (1985).
[20] F. Bueche, *Physical Properties of Polymers*, Wiley, New York, 1962, ch. 1.
[21] R.L. Jernigan and P.J. Flory, "Distribution functions for chain molecules," *J. Chem. Phys.*, **50,** 4185 (1969).
[22] D. Brown, "Vectorising your MD program for the Cyber 205 the Brode and Ahlrichs way," *Information Quarterly for Computer Simulation of Condensed Phases* (The CCP5 Newsletter), **24,** 39 (1987). This is an informal publication available on request from SERC Daresbury Laboratory, Warrington WA4 4AD, UK.
[23] S. Brode and R. Ahlrichs, "An optimized MD program for the vector computer Cyber 205," *Comp. Phys. Comm.*, **42,** 51 (1986).
[24] J. Rossignol, R. Seguela and F. Rietsch, "Mechanical behaviour of linear low density polyethylene fibres," *Polymer*, **29,** 43 (1988).
[25] I.M. Ward, *Mechanical Properties of Solid Polymers*, 2nd. Ed., Wiley, 1983, ch. 11.
[26] R. Popli and L. Mandelkern, "Influence of structural and morphological factors on the mechanical properties of the polyethylenes," *J. Poly. Sci.: Part B: Poly. Phys.*, **25,** 441 (1987).
[27] M. Parrish and N. Brown, "Yield phenomenon in oriented Polyethylene Terephthalate," in *Plastic Deformation of Polymers*, A. Peterlin, ed., Marcel Dekker, New York, 1971, pp. 189–209.
[28] D. Tabor, *Gases, liquids and solids*, Penguin, Glasgow, 1970, chs. 8 & 9.
[29] D. Brown and J.H.R. Clarke, "Constant-stress nonequilibrium molecular dynamics: Shearing of the soft-sphere crystal and fluid," *Phys. Rev. A*, **34,** 2093 (1986).
[30] W. Glenz and A. Peterlin, "Infrared studies of drawn Polyethylene. Part I. Changes in orientation and conformation of highly drawn linear Polyethylene," in *Plastic Deformation of Polymers*, A. Peterlin, ed., Marcel Dekker, New York, 1971, pp. 13–29.